J|A|C|S
ARTICLES
Published on Web 12/13/2003

Fluorescence Resonance Energy Transfer Between Quantum Dot Donors and Dye-Labeled Protein Acceptors

Aaron R. Clapp,[†] Igor L. Medintz,[‡] J. Matthew Mauro,[‡] Brent R. Fisher,[§] Moungi G. Bawendi,[§] and Hedi Mattoussi*,[†]

Contribution from the Optical Sciences Division, Code 5611, U.S. Naval Research Laboratory, Washington, D.C. 20375; Center for Bio/Molecular Science and Engineering, Code 6910, U.S. Naval Research Laboratory, Washington, D.C. 20375; and Department of Chemistry, Massachusetts Institute of Technology, Cambridge, Massachusetts 02139

Received July 5, 2003; E-mail: hedimat@ccs.nrl.navy.mil

Abstract: We used luminescent CdSe−ZnS core−shell quantum dots (QDs) as energy donors in fluorescent resonance energy transfer (FRET) assays. Engineered maltose binding protein (MBP) appended with an oligohistidine tail and labeled with an acceptor dye (Cy3) was immobilized on the nanocrystals via a noncovalent self-assembly scheme. This configuration allowed accurate control of the donor−acceptor separation distance to a range smaller than 100 Å and provided a good model system to explore FRET phenomena in QD−protein−dye conjugates. This QD−MBP conjugate presents two advantages: (1) it permits one to tune the degree of spectral overlap between donor and acceptor and (2) provides a unique configuration where a single donor can interact with several acceptors simultaneously. The FRET signal was measured for these complexes as a function of both degree of spectral overlap and fraction of dye-labeled proteins in the QD conjugate. Data showed that substantial acceptor signals were measured upon conjugate formation, indicating efficient nonradiative exciton transfer between QD donors and dye-labeled protein acceptors. FRET efficiency can be controlled either by tuning the QD photoemission or by adjusting the number of dye-labeled proteins immobilized on the QD center. Results showed a clear dependence of the efficiency on the spectral overlap between the QD donor and dye acceptor. Apparent donor−acceptor distances were determined from efficiency measurements and corresponding Förster distances, and these results agreed with QD bioconjugate dimensions extracted from structural data and core size variations among QD populations.

Introduction

Accurate and sensitive detection of water-soluble analytes, such as toxins, small molecule explosives, carbohydrates, ionic species, and various biomolecules including DNA, proteins, and peptides is a highly sought scientific goal with ramifications in healthcare, safety, and defense applications.[1−3] The interaction of a target molecule (e.g., analyte) with a protein receptor in a biological recognition process is often associated with a change in the protein conformation as a response to the binding event. Designing and developing recognition-based sensing assemblies that can account for such changes via a transduction signal in a medium of interest are the focus of many research groups.[4−6] Sensing studies utilizing Förster resonance energy transfer (FRET) between a fluorescent donor molecule bound to the target and an acceptor attached to a receptor protein have been widely used to study receptor−ligand interactions and changes in protein conformation upon binding to a target analyte or used as a response to changes in the solution conditions (e.g., temperature, pH conditions, etc.).[1,7] FRET is extremely sensitive to separation distance between the donor and acceptor and is ideal for probing such biological phenomena. Fluorescent organic molecules have been widely used as energy donors and acceptors in a variety of FRET-based biological studies.[7,8] They offer advantages such as small size, compatibility with numerous and simple covalent coupling strategies, and a relatively large detectable optical signal. While FRET has already been used extensively for biological applications, accurate measurements of time-dependent conformational change, such as monitoring protein dynamics over an extended period and continuous monitoring of target toxins or small molecule analytes under realistic constraints, remain difficult when using conventional

[†] Optical Sciences Division, Code 5611, U.S. Naval Research Laboratory.
[‡] Center for Bio/Molecular Science and Engineering, Code 6910, U.S. Naval Research Laboratory.
[§] Massachusetts Institute of Technology.

(1) Hermanson, G. T. *Bioconjugate Techniques*; Academic Press: London, 1996.
(2) Iqbal, S. S.; Mayo, M. W.; Bruno, J. G.; Bronk, B. V.; Batt, C. A.; Chambers, J. P. *Biosens. Bioelectron.* **2000**, *15*, 549−578.
(3) *Optical Biosensors: Present and Future*; Ligler, F. S., Rowe, C. A. Eds.; Elsevier: Amsterdam, The Netherlands, 2002.
(4) Benson, D. E.; Conrad, D. W.; de Lorimer, R. M., Trammell, S. A.; Hellinga, H. W. *Science* **2001**, *293*, 1641−1644.
(5) O'Connell, P. J.; Guilbault, G. G. *Anal. Lett.* **2001**, *34*, 1063−1078.
(6) Hellinga, H. W.; Marvin, J. S. *Trends Biotechnol.* **1998**, *16*, 183−189. Looger, L. L.; Dwyer, M. A.; Smith, J. J.; Hellinga, H. W. *Nature* **2003**, *423*, 185−190.
(7) Lakowicz, J. R. *Principles of Fluorescence Spectroscopy*, 2nd ed.; Kluwer Academic: New York, 1999.
(8) Turro, N. J. *Modern Molecular Photochemistry*; University Science Books: Mill Valley, CA, 1991.

organic dyes as the interacting donor−acceptor pair. Organic dyes often have narrow absorption spectra, broad emission with long tailing, and very low photobleaching thresholds, and they do not allow large Stokes shifts to be realized due to the small spectral separation between the absorption and emission peaks.[1,7] While the overall energy transfer may be efficient in these systems, there is often significant emission overlap that obscures the individual behavior of the donor and acceptor and leads to complications in the data analysis.[7,8] This is especially problematic in the development of "multichannel" assays where multiple analytes may be difficult to detect due to spectral cross talk.

Since the development of the synthetic reaction using high-temperature solution chemistry from organometallic precursors to prepare high quality colloidal semiconductor nanocrystals (quantum dots, QDs), and the advances that followed to improve and understand their photoemission properties, there has been increasing interest in understanding their fundamental physical properties and developing applications that take advantage of some of the unique features of these materials.[9−11] Goals include developing new materials such as quantum nanorods and magnetic nanocrystals,[12,13] designing and developing QD-based solar cells and light emitting devices (LEDs),[14−18] and recently addressing the large potential for using luminescent colloidal QDs as labeling reagents in biotechnological applications.[19−22] For biological tagging applications in particular, colloidal QDs have unique optical and spectroscopic properties that possess several inherent advantages over organic dyes and can offer a compelling alternative to traditional fluorophores in several fluorescence-based assay applications (e.g., fluoroimmuno and FRET-based assays). They show size dependent and tunable absorption and photoemission properties due to quantum confinement of the charge carriers (electron−hole pairs).[9−11,23,24] Their photoemission spectra are narrow and can be tuned over a broad region of the optical spectrum from near-UV to near-IR by either simple manipulation of the nanocrystal dimension for a given material composition and/or modification of the composition of the inorganic core used.[9−11,23,24] The broad tunable absorption properties permit simultaneous excitation of several QD populations while distinct emission characteristics of each population (size) are generated. The broad absorption spectra should allow flexibility in choosing the desired excitation wavelength in FRET studies where direct excitation of the acceptor molecules can be substantially reduced. Furthermore, advances in achieving surface passivation and additional confinement of the excitonic states by overcoating the native core with a wider band gap semiconductor improves the fluorescent quantum efficiency substantially, with resulting core−shell QDs having PL quantum yields comparable to those of organic dyes.[25−28]

Recently, several methods have been developed to disperse QDs in aqueous media for use in biologically relevant studies.[19−22,29,30] Functionalization of the water-soluble QD surface allows the formation of QD bioconjugates that can bind specifically to target molecules and form stable conjugate complexes. As such, QDs have already been used successfully in cellular imaging, immunoassays, DNA hybridization, and optical barcoding.[31−40]

We have previously demonstrated that engineered recombinant maltose binding proteins appended with an electrostatic attachment domain (MBP-zb) bind (via electrostatic self-assembly) irreversibly onto the surfaces of QDs capped with dihydrolipoic acid ligands.[21] This MBP-zb provided surface passivation while maintaining its maltose binding capability. We subsequently developed various fluorescence-based immunoassays that employed QDs conjugated only to MBP-zb or to a mixture of MBP-zb and another relevant protein, such as avidin, to prepare mixed surface QD−protein conjugates. This allowed the use of an MBP functionality to separate QD bioconjugates from unbound proteins over an amylose resin.[21,36,37,39]

In the present study, we have explored the potential of luminescent QD bioconjugates as fluorescent donors in a FRET-based assay. A cyanine dye (Cy3), serving as the energy acceptor, is covalently labeled to a recombinant maltose binding protein, and this dye−protein complex was immobilized on the nanocrystal surface. Using this configuration, we explored the

(9) Murray, C. B.; Norris, D. J.; Bawendi, M. G. *J. Am. Chem. Soc.* **1993**, *115*, 8706−8715.
(10) Qu, L.; Peng, Z. A.; Peng, X. *Nano Lett.* **2001**, *1*, 333−337.
(11) Gaponenko, S. V. *Optical Properties of Semiconductor Nanocrystals*; Cambridge University Press: Cambridge, 1998.
(12) Peng, X.; Manna, L.; Yang, W.; Wickham, J.; Scher, E.; Kadavanich, A.; Alivisatos, A. P. *Nature* **2000**, *404*, 59−61.
(13) Sun, S. H.; Murray, C. B.; Weller, D.; Folks, L.; Moser, A. *Science* **2000**, *287*, 1989−1992.
(14) Huynh, W. U.; Dittmer, J. J.; Alivisatos, A. P. *Science* **2002**, *295*, 2425−2427.
(15) Greenham, N. C.; Peng, X.; Alivisatos, A. P. *Phys. Rev. B* **1996**, *54*, 17628−17637.
(16) Schlamp, M. C.; Peng, X.; Alivisatos, A. P. *J. Appl. Phys.* **1997**, *82*, 5837−5842.
(17) Mattoussi, H.; Radzilowski, L. H.; Dabbousi, B. O.; Thomas, E. L.; Bawendi, M. G.; Rubner, M. F. *J. Appl. Phys.* **1998**, *83*, 7965−7974.
(18) Coe, S.; Woo, W. K.; Bawendi, M. G.; Bulovic, V. *Nature* **2002**, *420*, 800−803.
(19) Bruchez, M.; Moronne, M.; Gin, P.; Weiss, S.; Alivisatos, A. P. *Science* **1998**, *281*, 2013−2015.
(20) Chan, W. C. W.; Nie, S. *Science* **1998**, *281*, 2016−2018.
(21) Mattoussi, H.; Mauro, J. M.; Goldman, E. R.; Anderson, G. P.; Sundar, V. C.; Mikulec, F. V.; Bawendi, M. G. *J. Am. Chem. Soc.* **2000**, *122*, 12142−12150.
(22) Mattoussi, H.; Kuno, M. K.; Goldman, E. R.; Anderson, G. P.; Mauro, J. M. *Optical Biosensors: Present and Future*; Elsevier: Amsterdam, 2002; pp 537−569.
(23) Alivisatos, A. P. Semiconductor Clusters, Nanocrystals, and Quantum Dots. *Science* **1996**, *271*, 933−937.
(24) Efros, A. L.; Rosen M. *Annu. Rev. Mater. Res.* **2000**, *30*, 475−521.
(25) Hines, M. A.; Guyot-Sionnest, P. *J. Phys. Chem. B* **1996**, *100*, 468−471.
(26) Dabbousi, B. O.; Rodriguez-Viejo, J.; Mikulec, F. V.; Heine, J. R.; Mattoussi, H.; Ober, R.; Jensen, K. J.; Bawendi, M. G. *J. Phys. Chem. B* **1997**, *101*, 9463−9475.
(27) Peng, X.; Schlamp, M. C.; Kadavanich, A. V.; Banin, U.; Alivisatos, A. P. *J. Am. Chem. Soc.* **1997**, *119*, 7019−7029.
(28) Reiss, P.; Bleuse, J.; Pron, A. *Nano Lett.* **2002**, *2*, 781−784.
(29) Pathak, S.; Choi, S. K.; Arnheim, N.; Thompson, M. E. *J. Am. Chem. Soc.* **2001**, *123*, 4103−4104.
(30) Guo, W.; Li, J. J.; Wang, Y. A.; Peng, X. *J. Am. Chem. Soc.* **2003**, *125*, 3901−3909.
(31) Dubertret, B.; Skourides, P.; Norris, D. J.; Noireaux, V.; Brivanlou, A. H.; Libchaber, A. *Science* **2002**, *298*, 1759−1762.
(32) Jaiswal, J. K.; Mattoussi, H.; Mauro, J. M.; Simon, S. M. *Nat. Biotechnol.* **2003**, *21*, 47−51.
(33) Wu, X.; Liu, H.; Liu, J.; Haley, K.; Treadway, J. A.; Larson, J. P.; Ge, N.; Peale, F.; Bruchez, M. P. *Nat. Biotechnol.* **2003**, *21*, 41−46.
(34) Akerman, M. E.; Chan, W. C. W.; Laakkonen, P.; Bhatia, S. N.; Ruoslahti, E. *Proc. Natl. Acad. Sci. U.S.A.* **2002**, *99*, 12617−12621.
(35) Han, M.; Gao, X.; Su, J. Z.; Nie, S. *Nat. Biotechnol.* **2001**, *19*, 631−635.
(36) Tran, P. T.; Goldman, E. R.; Anderson, G. P.; Mauro, J. M.; Mattoussi, H. *Phys. Status Solidi B* **2002**, *229*, 427−432.
(37) Goldman, E. R.; Anderson, G. P.; Tran, P. T.; Mattoussi, H.; Charles, P. T.; Mauro, J. M. *Anal. Chem.* **2002**, *74*, 841−847.
(38) Gerion, D.; Parak, W. J.; Williams, S. C.; Zanchet, D.; Micheel, C. M.; Alivisatos, A. P. *J. Am. Chem. Soc.* **2002**, *124*, 7070−7074.
(39) Goldman, E. R.; Balighian, E. D.; Mattoussi, H.; Kuno, M. K.; Mauro, J. M.; Tran, P. T.; Anderson, G. P. *J. Am. Chem. Soc.* **2002**, *124*, 6378−6382.
(40) Xu, H.; Sha, M. Y.; Wong, E. Y.; Uphoff, J.; Xu, Y.; Treadway, J. A.; Truong, A.; O'Brien, E.; Asquith, S.; Stubbins, M.; Spurr, N. K.; Lai, E. H.; Mahoney, W. *Nucleic Acids Res.* **2003**, *31*, e43.

effects of varying the ratio of dye-labeled proteins attached to the QDs while maintaining a fixed total number of proteins in a QD conjugate. Furthermore, we altered the degree of spectral overlap between the donor and acceptor (by tuning the nanocrystal size, thus, the emission location for a fixed acceptor dye) and examined its effect on the FRET efficiency in these systems. In particular, we found that when the QD dimensions changed, the measured rate of FRET can be substantially affected even for the same dye acceptor, with better overlap providing enhanced transfer efficiency. We also found that the measured FRET efficiency for a fixed acceptor dye increased substantially with increasing number of dye-labeled proteins during a titration sequence. This results from progressive quenching of the QD emission and subsequent enhancement of the dye PL signal with increasing number of dye-labeled proteins immobilized on the QD surface. These observations have been confirmed by fluorescence lifetime measurements, where a substantial shortening of the QD donor lifetime was measured in the presence of dye-labeled proteins. Analysis of the above set of data using the Förster model yielded accurate estimates for the separation distances for various QD−dye pairs studied. Deriving the donor−acceptor (D−A) separation distance for the configuration of a QD conjugate interacting with several acceptors provided a statistical estimate for the QD−protein spatial extension as multiple values could be extracted for the same D−A pair and compared. These results demonstrate the utility of using QDs as energy donors and lay the groundwork for the design and implementation of QD-based nanoscale biosensors using FRET.

Background: Förster Energy Transfer Formalism

Fluorescence (or Förster) resonance energy transfer (FRET) is a process that involves nonradiative energy transfer from a photoexcited donor molecule, after absorption of a higher energy photon, to an acceptor molecule of a different species (brought in close proximity), which may relax to its ground state by emitting a lower energy photon. This process results from dipole−dipole interactions and is thus strongly dependent on the center-to-center separation distance; it requires a nonzero integral of the spectral overlap between donor emission and acceptor absorption.[7] Careful selection of an appropriate donor−acceptor pair ensures high transfer efficiency and provides two measurable parameters: a quenched donor photoemission and enhanced acceptor fluorescence. While good spectral overlap is paramount to high transfer efficiency, the donor and acceptor photoluminescence (PL) signals must also be well resolved to extract accurate experimental information for the system under investigation, e.g., a binding event due to a specific interaction in a biological receptor−ligand system or a change in protein conformation due to interactions with a target molecule. In addition, the excitation line should be chosen to coincide with the minimum of the acceptor absorption spectrum in order to reduce contributions resulting from direct excitation of the acceptor. Satisfying all of these conditions simultaneously is inherently difficult using conventional organic dyes with narrow excitation spectra and small achievable Stokes shifts.

The rate of energy transfer for an isolated single D−A pair separated by a distance r can be expressed using the Förster formalism as[7,8]

$$k_{D-A} = \frac{B \times Q_D I}{\tau_D r^6} = \left(\frac{1}{\tau_D}\right) \times \left(\frac{R_0}{r}\right)^6 \quad (1)$$

where Q_D is the quantum yield of the donor and τ_D is the excited-state lifetime of the donor; the constant B is a function of the refractive index of the medium n_D, Avogadro's number N_A, and a parameter, κ_p, that depends on the relative orientation of the donor and acceptor dipoles:[7,8]

$$B = \frac{[9000 \times (\ln 10)]\kappa_p^{\,2}}{128\pi^5 n_D^{\,4} N_A} \quad (2)$$

where $\kappa_p^2 = {}^2/_3$ for randomly oriented dipoles and varies between 0 and 4 for the cases of orthogonal and parallel dipoles, respectively. The overlap integral, I, defined as

$$I = \int_0^\infty PL_{D-corr}(\lambda)\epsilon_A(\lambda)\lambda^4 \, d\lambda \quad (3)$$

is a quantitative measure of the donor−acceptor spectral overlap over all wavelengths λ; it is a function of the normalized donor emission spectrum (dimensionless property), PL_{D-corr}, and the acceptor absorption spectrum (expressed as an extinction coefficient), ϵ_A. In eq 1, we introduced the Förster radius (or distance), R_0, which is defined as

$$R_0 = (BQ_D I)^{1/6} = \left(\frac{9000(\ln 10)\kappa_p^{\,2} Q_D}{N_A 128\pi^5 n_D^{\,4}} I\right)^{1/6} \quad (4)$$

and corresponds to a separation distance at which the rate of transfer matches the rate of exciton decay: $k_{D-A} = \tau_D^{-1}$. Note that the quantum yield must be measured to give an accurate estimate of the Förster distance. The FRET efficiency, E, defined as

$$E = \frac{k_{D-A}}{k_{D-A} + \tau_D^{-1}} = \frac{R_0^{\,6}}{R_0^{\,6} + r^6} \quad (5)$$

accounts for the fraction of excitons that are transferred from the donor to the acceptor nonradiatively. Using eq 5 for the FRET efficiency, one can also define the Förster distance, R_0, as the separation distance that yields 50% energy transfer efficiency. In the case where one donor species can interact with several acceptors brought in close proximity simultaneously, the above analysis can be modified to account for the presence of these complex interactions, and the above efficiency can be expressed as

$$E = \frac{nR_0^{\,6}}{nR_0^{\,6} + r^6} \quad (6)$$

where n is the average number of acceptor molecules interacting with one donor. In the above configuration the presence of several acceptor fluorophores increases the rate of FRET. It may be described as an effective linear enhancement of the energy transfer cross section between a donor and several acceptors arrayed around its center (e.g., a QD−protein−dye bioconjugate complex as depicted in Figure 1).

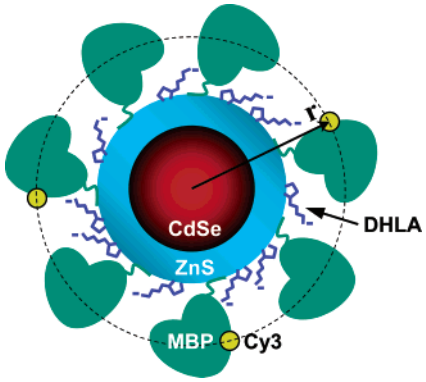

Figure 1. Schematic representation of the QD−MBP−dye nanoassembly (bioconjugate, not drawn to scale) used. In this study, we limited the total number of proteins immobilized on each QD surface to ∼15. The distance *r* represents the radius or average distance between the QD center and location of the Cy3-labeled residue on MBP.

The FRET efficiency can be measured experimentally and is commonly defined as[7]

$$E = 1 - \frac{F_{DA}}{F_D} \tag{7}$$

where F_{DA} is the integrated fluorescence intensity of the donor in the presence of the acceptor(s) and F_D is the integrated fluorescence intensity of the donor alone (no acceptors present). Equations 6 and 7 can be combined to provide an expression for the donor−acceptor separation distance for each number *n*

$$r_n = \left(\frac{nR_0^6(1-E)}{E}\right)^{1/6} = R_0\left(\frac{n(1-E)}{E}\right)^{1/6} \tag{8}$$

which can be experimentally determined from fluorescence data. It can provide quantitative information about specific binding events in a bioconjugate, including the case where *n* acceptors are brought in close proximity to a single donor as a result of these specific interactions. The above configuration applies to our QD bioconjugates, where a QD donor can interact with several acceptor dyes that have been covalently attached to the proteins immobilized on the surface to form a QD−protein−dye complex.

The above treatment of QD-based FRET with an acceptor dye using the Förster analysis assumes an exciton with a symmetric wave function around the nanocrystal center, which may not be appropriate.[11,24] The Förster theory treats the donor and acceptor as points in the interaction space, whereas the nanocrystals have finite size and are relatively large compared to the dye molecules.[42] Nonetheless, this treatment is the best available for the present scenario.

Materials and Methods

Quantum Dot Synthesis. We used CdSe−ZnS core−shell QDs prepared using established synthetic techniques consisting of growth and annealing of organometallic precursors at high temperature, as described elsewhere.[9,10,25,26] Briefly, CdSe−ZnS core−shell nanoparticles capped with a mixture of trioctyl phosphine/trioctyl phosphine oxide (TOP/TOPO) ligands were prepared using a stepwise procedure that consists of CdSe core growth and annealing of organometallic precursors in a high-temperature coordinating solution made of TOP/TOPO mixed with additional amine terminated ligands, followed by overcoating the native core with a thick layer of ZnS (consisting of ∼5−7 monolayers), also carried out in a high-temperature coordinating mixture; ZnS overcoating is usually carried out at temperatures lower than those used during CdSe nanocrystal growth to avoid compromising the integrity of the native cores. Robust nanocrystals with narrow size distribution, symmetric photoemission spectra (fwhm of 30−40 nm), and high photoluminescence quantum yields (QY) are prepared using this synthetic approach. Three QD samples having PL emission maxima at 510, 530, and 555 nm were synthesized and used in this study. The resulting CdSe−ZnS core−shell QDs were rendered water soluble by replacing the native TOP/TOPO organic capping shell with bidentate dihydrolipoic acid (DHLA, a dithiol-alkyl-COOH) ligands, as described previously.[21] This provided aggregate-free water-soluble QD preparations with good quantum yields and which were exceptionally stable in basic pH buffer. DHLA-capped CdSe−ZnS QD samples (∼10−40 μM) stable over a period of 1 year have been routinely prepared in our laboratory. The DHLA-capped nanocrystals have a homogeneous density of charge due to deprotonation of the carboxylic acid end groups. The relatively long term stability is presumably due to the strong bidentate interactions of the DHLA ligands with the ZnS surface via their dithiol polar heads in comparison, for example, with monothiol terminated caps.[21]

Protein Engineering. Maltose binding protein was engineered to express a short oligohistidine sequence (consisting of five histidine amino acids) at its C-terminus. This histidine-terminated MBP (MBP-his) can effectively and tightly bind to DHLA-capped QDs. Conjugation via the oligohistidine attachment resulted in the observed progressive enhancement of the QD conjugate QY upon increasing number of MBP-his conjugated to each nanoparticle, with saturation occurring when the number of proteins reached a maximum allowed by steric limitations of packing around a nanocrystal.[21] We anticipate that this conjugation process is driven by specific recognition of the oligohistidine element to the ZnS/DHLA on the CdSe−ZnS QDs.[42]

In this study, we used histidine-terminated MBP, labeled prior to immobilization on the QD surfaces with an organic dye (Cy3), which is covalently attached to a unique residue, to carry out our FRET investigation. Additional details that describe the protein preparation are reported elsewhere.[42,43] The MBP variant used in the present FRET studies was engineered to express a cysteine residue at position 95, replacing the usual aspartic acid residue (MBP95C-his, asp-95 → cys-95).[43] Monofunctional maleimide Cy3 purchased from Amersham Pharmacia (Piscataway, NJ) was used to specifically label the D95 residue of the MBP-his. For labeling, the protein was reduced with Cleland's Reductacryl Reagent (Calbiochem, San Diego, CA) and then mixed with the activated dye. This procedure permitted an average labeling ratio of 1.0 Cy3/MBP, as deduced from the extinction coefficients of the protein at 280 nm and the dye at 553 nm (measured using a UV/visible spectrophotometer, model 8453, Hewlett-Packard, Palo Alto, CA). Cy3-labeled MBP-his proteins were purified by column chromatography using P-6 or PD-10 columns (Amersham Pharmacia) to remove excess unreacted dye.

QD−Protein Conjugate Preparation. Bioconjugate complexes were prepared by adding appropriate amounts of Cy3-labeled and unlabeled MBP to 100 μL of 10 mM sodium tetraborate buffer solution (pH 9). Approximately 24 pmol of DHLA capped QDs were added to the MBP solution and allowed to self-assemble for ∼15 min at room temperature. Molar ratios of MBP−Cy3 to QDs were discretely varied among samples from 0 to 10 while the overall ratio of MBP (labeled and unlabeled) to QD was maintained at 15 (see sketch in Figure 1). The individual samples were then diluted with sodium tetraborate buffer to a total volume of 3 mL. The solutions were placed in a 10 mm

(41) Kagan, C. R.; Murray, C. B.; Bawendi, M. G. *Phys. Rev. B* **1996**, *54*, 8633.
(42) Medintz, I. L.; Clapp, A. R.; Mattoussi, H.; Goldman, E. R.; Mauro, J. M. *Nat. Mater.* **2003**, *2*, 630−638.
(43) Medintz, I. L.; Goldman, E. R.; Lassman, M. E.; Mauro, J. M. *Bioconjugate Chem.* **2003**, *14*, 909−918.

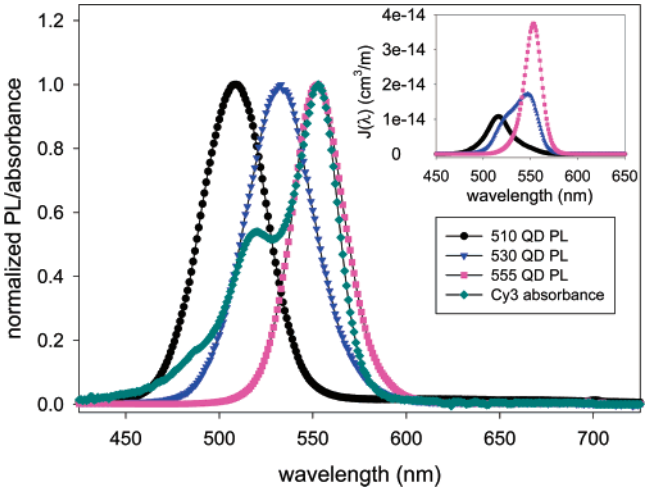

Figure 2. Normalized absorption spectra (ϵ_A) of Cy3 dye and photoemission spectra of the three CdSe−ZnS core−shell QD solutions. Inset shows plots of the resulting overlap functions, $J(\lambda) = PL_{D-corr}(\lambda) \times \lambda^4 \times \epsilon_A(\lambda)$, and highlights the effects of size tuning the QD emission on the degree of spectral overlap for a given acceptor dye (Cy3).

optical path quartz fluorescence cuvette (FUV, Spectrocell, Oreland, PA), and the emission spectra were measured using a SPEX Fluorolog-2 fluorimeter (Jobin Yvon/SPEX, Edison, New Jersey). All samples were excited at 430 nm, which is near the minimum of the Cy3 absorption spectrum in order to reduce interference from direct excitation of the acceptor (see Figure 2).

Furthermore, control spectra collected from MBP−Cy3 conjugates in the absence of QD donors were recorded and subtracted from the solution spectra to adjust for dye emission exclusively due to direct excitation. To avoid inner filtering effects, QD conjugate preparations with optical density (OD) at the excitation line below 0.05 were used in all experiments.

Estimate of the Number of Proteins per QD−MBP-his Conjugate. Cy3-labeled MBP-his was utilized to measure the MBP concentration in the QD conjugate solution by monitoring the absorption of Cy3 dye at 553 nm (peak of the absorption spectrum, see Figure 2). This is better and more accurate than using the protein absorption at 280 nm, where interference from the large nanocrystal absorption could provide erroneous results. Experimentally, QDs (e.g., 555 nm emitting nanocrystals) were mixed with the molar amount of MBP95C−Cy3 necessary to form QD conjugates with the targeted number of proteins and allowed to self-assemble for ∼15 min; a control solution with pure MBP95C−Cy3 (no QDs) was also prepared. The two solutions contained the same amounts of proteins as checked by the comparable absorbance at 553 nm. The conjugate and control solutions were loaded onto an Amicon Centricon spin dialysis tube having a cutoff molecular weight, MW, of 100 kDa (larger than the estimated protein MW of ∼45 kDa) and centrifuged at 1000 × *g* 2 times for 20 min each, with a borate buffer wash between the spins. The amount of dye-labeled MBP in the dialysate was extracted for each solution from the absorbance at 553 nm. More than 95% of the protein in the control sample passed through the membrane, whereas negligible (less than 3%) dye-labeled MBP95C was collected in the dialysate for the sample containing the QD conjugates. The QDs conjugated to 10 or more MBP95C−Cy3 with a MW of ∼500 kDa or larger are blocked by the membrane. This result implies that essentially all the proteins added self-assembled onto the nanocrystal surface to form stable Cy3-labeled QD−MBP95C conjugates.[42] Verification of the number of MBP-his per QD conjugate was derived from QD PL enhancement with increasing number of proteins immobilized on each QD surface as reported in refs 21 and 42. Further proof for QD−MBP conjugate formation as well as an estimate of the number of proteins per conjugate is provided by the FRET data, which will be presented below.

Table 1. Overlap Integrals, Quantum Yields, and Calculated Förster Distances for MBP-Coated QD−Cy3 Pairs

donor–acceptor pair	overlap integral, $I \times 10^{13}$ (cm³/M)	quantum yield,[a] Q_D	Förster distance, R_0 (Å)
510−Cy3	3.86	0.190	47.3
530−Cy3	7.01	0.153	50.4
555−Cy3	8.91	0.239	56.5

[a] Quantum yield of conjugates with 15 MBP per QD.

Fluorescence Lifetime Measurements. Fluorescence lifetimes were measured using a custom-built far-field epifluorescence microscope coupled to a spectrometer and time-gated intensified charge-coupled device (CCD) camera (Imager QE, LaVision GmbH, Göettingen, Germany). The microscope setup permitted use of very small excitation powers (∼30 μW) while maintaining a strong photoemission signal. The excitation light source was coupled to the microscope collection axis using a 400 nm dichroic filter and a 0.3 NA 10× objective (Nikon, Tokyo, Japan) placed after the dichroic filter was used to focus the excitation light onto the sample and collect the emitted fluorescence signal. An additional long pass filter inserted after the dichroic mirror was used to eliminate residual signal from the laser line and transmit only relevant (PL) signals onto the CCD detector. A pulsed GaN diode laser (414 nm, 5 MHz, 90 ps full width at half-maximum, model LDH400, PicoQuant GmbH, Berlin, Germany) was used to excite the sample. The overall instrument response time was limited to 500 ps by the CCD image intensifier microchannel plate. Data were collected at room temperature using a 10 mm optical path fluorescence cell filled with 3 mL of QD conjugates in buffer solution, as described above. Raw intensity data were obtained as functions of time and wavelength using DaVis software (LaVision GmbH).

Results

QD−MBP−Cy3 Titrations. Figure 2 shows the absorption spectrum of the Cy3 dye and emission spectra of the three QD solutions (spectra are normalized), along with plots of the overlap function for the QD−dye pairs used in this study. Table 1 shows the calculated overlap integrals, *I*, and Förster distances, R_0, for the various QD−dye pairs using eq 4 and the experimental values for Q_D, n_D, and a value of $^2/_3$ for κ_p^2; this characterizes a random distribution of dipoles, which is justified in this system due to the partially random orientation of the QD dipole, random packing of MBP around the QD surface, and a random orientation of the dye dipole within the MBP structure.

Quantum yield measurements are reported for QDs conjugated to 15 MBPs and used in the calculation of R_0 values. The plots shown in Figure 2 and values reported in Table 1 clearly indicate that the degree of spectral overlap between the QD donors and Cy3 acceptor varies as a function of the emission location for each QD population; it further confirms the anticipated ability of controlling the degree of spectral overlap by simply tuning the nanocrystal size (i.e., its photoemission spectrum). This property benefited from the narrow and nearly Gaussian distribution of the individual QD PL spectra.

Figure 3A−C show the PL spectra of the QD donor and Cy3 dye acceptor for each ratio *n* (in a titration series where increasing amounts of MBP−Cy3 are substituted for unlabeled MBP within each conjugate) for the three sets of QD−dye pairs used.

In all cases, raw PL spectra were corrected to account for direct excitation of the acceptor and deconvoluted to provide separate signals characteristic of the QD and Cy3 fluorophores. Although acceptor absorption was minimized by selecting an

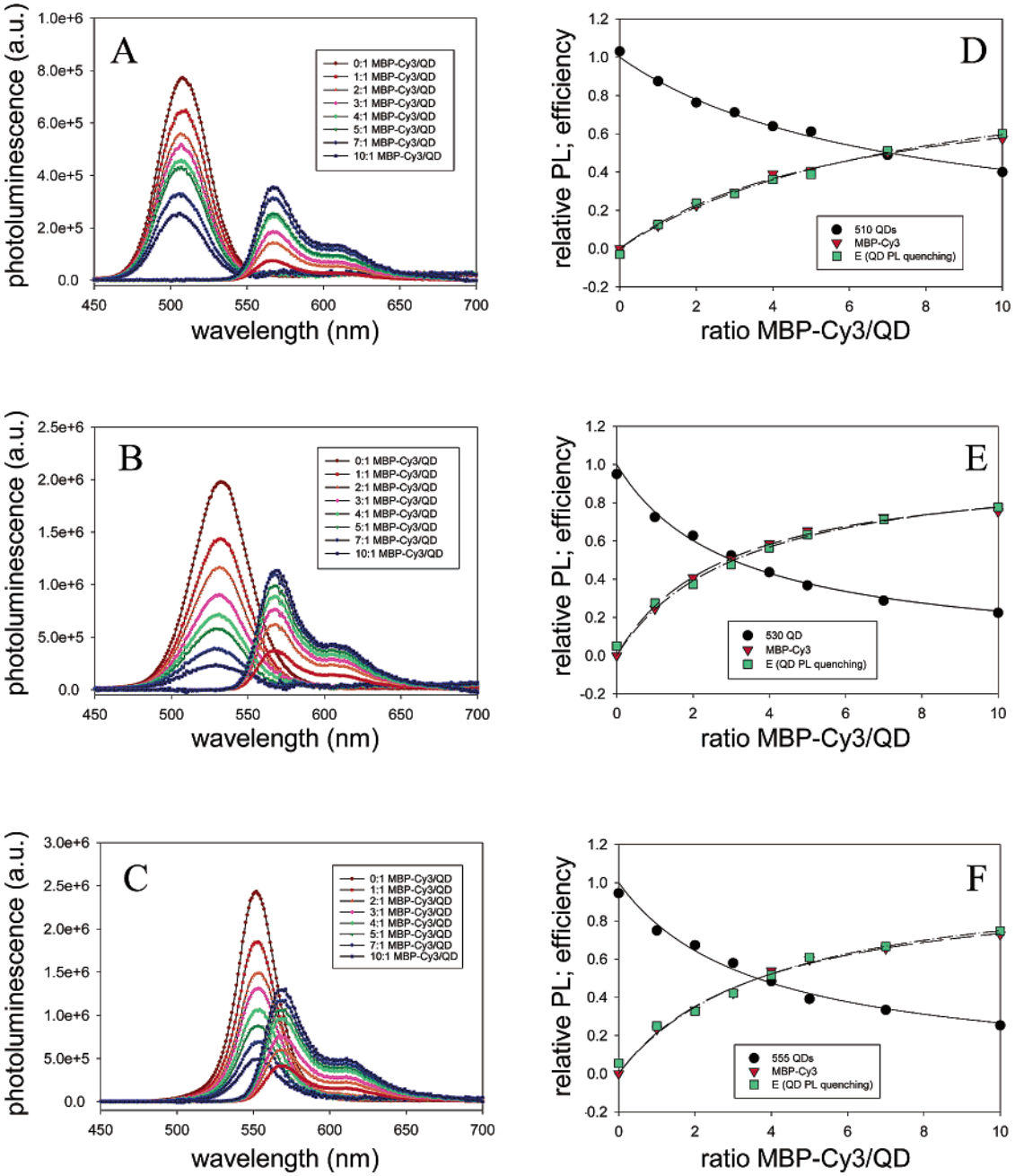

Figure 3. (A−C) Evolution of the photoluminescence spectra from the QDs and Cy3 dyes in the QD−MBP−Cy3 assemblies versus increasing dye-to-QD ratio *n*, after deconvoluting the raw signal and subtracting the contribution due to direct excitation of the acceptor ((A) 510 nm emitting QDs, (B) 530 nm emitting QDs, and (C) 555 nm emitting QDs). The total number of proteins per QD conjugate was fixed. (D−F) Experimental values for the donor PL decay percentage (●) versus *n* together with a fit to a hyperbolic function complementary to eq 6 (solid line), the rate of FRET extracted for the donor PL loss (▼) together with a fit to eq 6 (dashed line), and the rate of FRET deduced from acceptor gain (■) together with a fit using eq 6 (dash−dotted line). Figure 3D, E, and F correspond to 510, 530, and 555 nm QDs, respectively.

excitation at 430 nm (within the valley of Cy3 absorption spectrum, see Figure 2), appreciable PL signal due to direct excitation was measured in all cases. Deconvolution of the composite signal was performed by assuming a linear superposition of PL signals with known shapes, yielding individual spectra for QDs and dye for each ratio *n*. The data show that there is a clear progression in the fluorophore emissions as a function of increasing number of MBP−Cy3 substituted for unlabeled proteins, namely a progressive quenching of the QD emission and a systematic enhancement of the Cy3 emission as the number of dyes surrounding the QD increased from 0 to 10.

Figure 3D−F depict the integrated PL signals for the three sets of solutions used, 510, 530, and 555 nm emitting QDs (shown in Figure 3A−C), as a function of the Cy3/QD ratio. In addition, a fit to a hyperbolic function of the form expressed in eq 6 is shown for all three sets. All other relevant parameters (namely the separation distance *r*) should be unaffected during the titration experiment. The fits agree well with the experimental observations for the progressive donor quenching compared to acceptor PL enhancement with increasing number of MBP−Cy3 immobilized on a single QD. We also reported the values for the expected acceptor integrated PL intensity extracted from the FRET efficiency, using eq 7 for *E* (squares

Table 2. Fluorescence Lifetime Measurements of QDs

bound species	510 QD lifetime, τ (ns)	530 QD lifetime, τ (ns)	555 QD lifetime, τ (ns)
10MBP/0MBP−Cy3	2.72 ± 0.15	3.19 ± 0.07	2.51 ± 0.15
9MBP/1MBP−Cy3	2.59 ± 0.12	2.38 ± 0.24	2.08 ± 0.21
8MBP/2MBP−Cy3		1.78 ± 0.12	
7MBP/3MBP−Cy3	2.03 ± 0.10	1.44 ± 0.12	1.17 ± 0.30
5MBP/5MBP−Cy3	1.60 ± 0.08	1.09 ± 0.12	1.18 ± 0.20
3MBP/7MBP−Cy3	1.47 ± 0.32	0.95 ± 0.04	1.35 ± 0.02
0MBP/10MBP−Cy3	1.08 ± 0.08	0.84 ± 0.03	1.01 ± 0.04

in Figure 3D−F), and compared them directly to the fractional integrated PL of the dye (triangles). In all cases, the trends are consistent as a progressive increase in the acceptor emission follows the expected energy gain. These results strongly suggest that FRET is the primary mechanism for the reported observations.

Fluorescence Lifetimes. Nonradiative exciton transfer is also expected to substantially alter the exciton lifetime properties of the donor. In particular, a comparison between measurements of the exciton lifetimes of the donor alone and the donor interacting with an acceptor molecule brought in close proximity, τ_D and τ_{DA}, respectively, should provide information on the FRET efficiency for the present set of samples and conditions. To investigate this phenomenon in the context of our study, we carried out exciton lifetime measurements for all three samples of QDs conjugated to varying ratios of MBP−Cy3/QD. These values were compared to a reference consisting of QD−MBP conjugates with no Cy3 labeled protein (Table 2).

QD fluorescence intensity was integrated over a range of wavelengths representative of donor-only emission and plotted as a function of time. Figures 4A and 5A show representative plots for the QD fluorescence intensity decay with time for selected dye-labeled MBP to QD ratios for 510 and 530 nm emitting QD conjugates; similar data were collected for solutions of the 555 nm QD−MBP−Cy3 pair. There is a clear difference in the donor fluorescence decay time as an increasing ratio of MBP−Cy3 was substituted in the QD conjugates, with shorter decay times observed for larger Cy3/QD ratios. To extract values for the exciton decay time τ, a fit of the fluorescence decay data to a biexponential function of the type $I(t) = a \exp(-\alpha t) + b \exp(-\beta t)$ was used instead of a stretched exponential[44] because it provided better agreement with the present QD−MBP−Cy3 data (see Figures 4A and 5A). Furthermore, because the best fit corresponded to $b/a < 1$, the first decay constant was used to extract a value for the exciton lifetime, $\tau = \alpha^{-1}$, for all samples and reported in Table 2.

Using the raw spectroscopic data, we generated time-series images of the fluorescence signals following an excitation laser pulse. Figures 4B−D and 5B−D each display three series of four image (false color time-intensity-wavelength) frames taken at 2 ns intervals, where pixels along the abscissa axis designate wavelength progression, the ordinate axis is pixel position, and PL intensities are reported as color contours. Figure 4 corresponds to 510 nm emitting QDs, whereas Figure 5 corresponds to 530 nm emitting QDs. For clarity, the QD and Cy3 emission maxima are indicated with dashed lines. Figures 4B and 5B depict data from QDs coated with 10 MBP, seven of which were Cy3-labeled. Figures 4C and 5C show data from QDs coated with 10 unlabeled MBP. Last, Figures 4D and 5D show data from free MBP−Cy3 equivalent in concentration to 10 MBP−Cy3/QD.

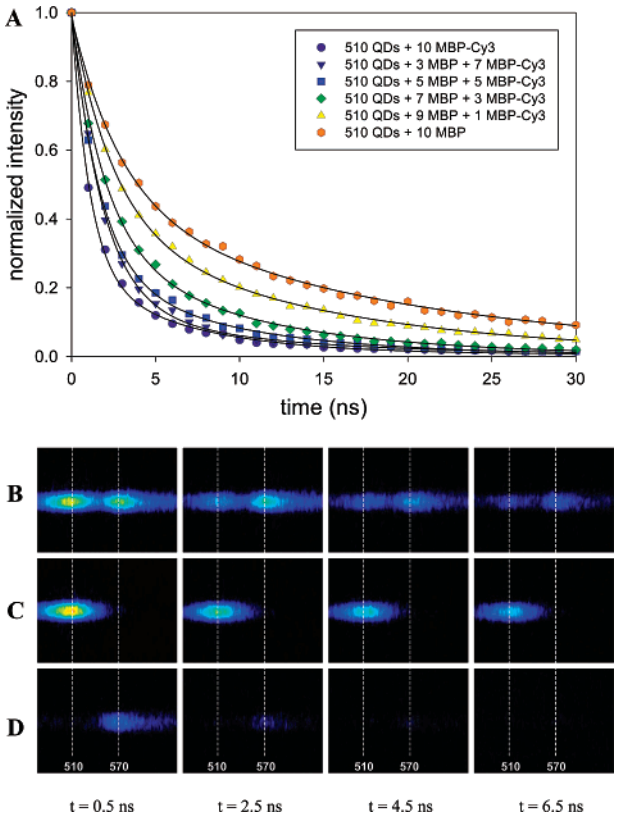

Figure 4. (A) Plot of the 510 nm emitting QD photoemission intensity versus time immediately after a short pulse excitation signal. Data are shown for various QD−MBP−Cy3 conjugate configurations where the number of Cy3-labeled proteins was increased from 0 to 10, while maintaining the total number of proteins fixed at 10 MBP/QD. (B−D) Series of images showing the intensity of (B) 510 nm QDs with 3 MBP/7 MBP−Cy3, (C) 510 nm QDs with 10 MBP per QD, and (D) free MBP−Cy3 equivalent to 10 MBP−Cy3 per QD (no QDs present) as recorded by the CCD camera at 2 ns intervals.

Clearly, when MBP−Cy3 was immobilized on the QD surface, the fluorescence lifetime was noticeably shortened. The image sequence corresponding to a QD−MBP−Cy3 complex shows a near complete quenching of the QD emission following the initial three frames (within the initial 6.5 ns) for the 510 nm emitting QD donors; a total quenching of the QD emission occurs within 5 ns for solutions of the 530 nm emitting QDs. Comparison of the Cy3 signal in the presence and absence of QD donors shows clearly differing behavior. Without QDs present, the Cy3 direct excitation is very small (at 414 nm) and the lifetime is relatively short. These results are a direct product of an efficient FRET process between the QD donors and Cy3 acceptors and further reflect the subtle differences in the integral overlap between the two systems; 510 nm emitting QDs provide a weaker overlap with Cy3 than 530 nm nanocrystals and thus experience a slightly slower quenching in the presence of the dye acceptor.

Discussion

The set of data presented above, in particular the PL behavior depicted in Figure 3 and the substantial shortening in the QD exciton lifetime upon conjugate formation (shown in Figures 4 and 5), indicate conclusively that efficient FRET occurs between

(44) Lindsey, C. P.; Patterson, G. D. *J. Chem. Phys.* **1980**, *73*, 3348−3357.

Table 3. Comparison of Measured Donor−Acceptor Distances Using Various Estimates of Efficiency

ratio Cy3/QD, *n*	measured donor–acceptor distance, r_n (Å)								
	510 QD–Cy3			530 QD–Cy3			555 QD–Cy3		
	QD PL[a]	QD lifetime[b]	Cy3 PL[c]	QD PL[a]	QD lifetime[b]	Cy3 PL[c]	QD PL[a]	QD lifetime[b]	Cy3 PL[c]
1	65.2	64.2	66.0	61.2	60.3	60.7	67.8	74.0	68.9
2	64.4		65.2	63.1	58.8	60.1	71.5		71.0
3	66.0	64.1	65.7	62.6	58.5	60.3	71.5	75.4	71.4
4	65.5		64.1	61.7		59.9	70.3		69.3
5	66.7	63.1	65.7	60.9	59.0	59.2	68.5	74.5	69.1
7	64.9	64.8	65.2	60.6	60.4	59.3	69.6	76.7	70.2
10	64.8	63.0	66.0	60.8	62.3	61.4	69.2	74.7	70.3
$<r_n>$[d]	65.4 ± 0.8	63.9 ± 0.8	65.4 ± 0.7	61.6 ± 1.0	59.9 ± 1.4	60.1 ± 0.8	69.8 ± 1.4	75.0 ± 1.0	70.0 ± 1.0
r[e]		65−66			67−68			70−71	

[a] Estimated using QD PL quenching data (eq 7). [b] Estimated using QD fluorescence lifetime data (eq 9). [c] Estimated using Cy3 PL enhancement (eq 10) [d] Reported errors are standard deviations of the experimental measurements. [e] Estimated from QD radius using SAXS and TEM (refs 26, 45, and 46).

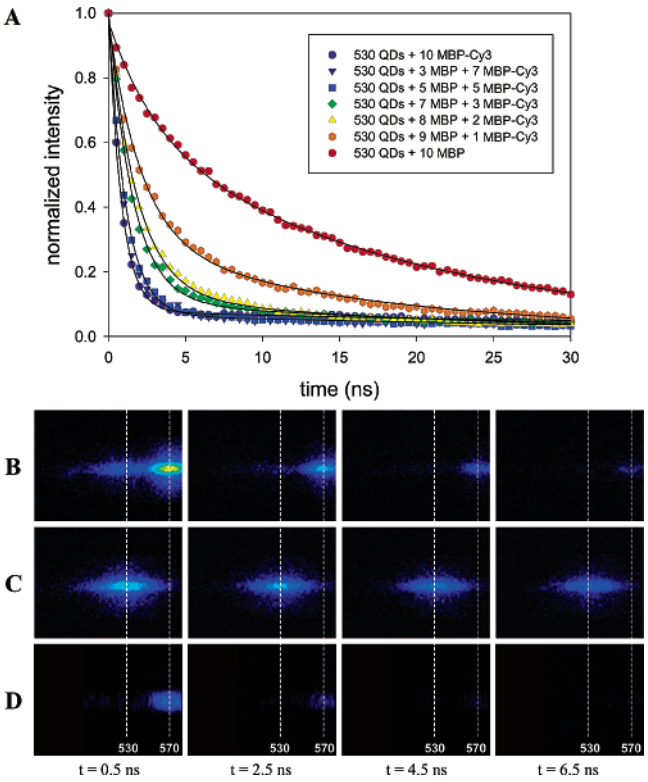

Figure 5. (A) Plot of the 530 nm emitting QD photoemission intensity versus time immediately after a short pulse excitation signal. Data are shown for various QD−MBP−Cy3 conjugate configurations where the number of Cy3-labeled proteins was increased from 0 to 10, while maintaining the total number of proteins fixed at 10 MBP/QD. (B−D) Series of images showing the intensity of (B) 530 nm QDs with 3 MBP/7 MBP−Cy3 per QD, (C) 530 nm QDs with 10 MBP per QD, and (D) free MBP−Cy3 equivalent to 10 MBP−Cy3 per QD (no QDs present) as recorded by the CCD camera at 2 ns intervals.

a QD donor placed at the center of a three-dimensional nanoscale conjugate assembly with Cy3 dyes distributed at a presumably fixed distance from the QD center. Furthermore, the efficiency is strongly dependent on the QD donor emission location, with highest FRET efficiency observed for 555 nm emitting QDs and weakest recorded for dots emitting at 510 nm. This result is consistent with the difference in the degree of spectral overlap among the set of donor−acceptor pairs investigated. For instance, comparison between the extreme cases indicates that the overlap integral I is ∼2 times larger for the pair 555 nm QD−Cy3 than the one for 510 nm QD−Cy3 (see Figure 2 and Table 1). This property confirms our ability to tune the degree of spectral overlap between donor and acceptor by simply changing the QD population used. It is worth emphasizing that tuning the nanocrystal photoemission location is accomplished via size control, which in turn affects the separation distance and thus the rate of FRET in these QD conjugates.

Using the conventional definition of FRET efficiency as the fractional loss in donor photoemission (i.e., donor quenching, eq 7) upon nonradiatively interacting with one or more acceptors and the relation between r and n, we extracted experimental estimates for the center-to-center separation distance for each ratio n (see Table 3).

Compilation of all values for each QD−Cy3 pair provided an average distance with a statistical error; the mean distances and standard deviations are also listed in Table 3. Note that these calculations depend on two measured parameters: PL quantum yield of the donor, Q_D, and the overlap integral I. The former is particularly important since it can vary with the nanocrystal size and between samples, and it must be measured against a well-characterized standard. In this study, we determined the quantum yield of the QDs against rhodamine 6G in ethanol (Q_{R6G} = 95%).[42] In addition, because the QD PL increases significantly (by values between 50 and 150%) upon protein binding for our QD−protein conjugates), the quantum yields used in the analysis (Q_D) were proportionally adjusted to account for the observed increase.[7,21,26]

Even though the extracted values for r listed in Table 3 are consistent within the same series, only comparison to those estimated from geometrical considerations that take into account the experimental radius of the QD, the protein dimensions, and protein packing around the nanocrystals would validate the above analysis and could provide an insight into the understanding of which relevant parameters affect the FRET process and its efficiency. The distances reported in Table 3 are in agreement with those deduced from geometrical considerations for the 555 nm QD and Cy3 pair. In particular, estimates of the core−shell nanocrystal radius from small-angle X-ray scattering (SAXS) and TEM experiments indicate that, for QDs emitting at 555 nm overcoated with about five monolayers of ZnS, the overall radius is ∼30−31 Å and a spatial extension of the 95C residue on the protein (where Cy3 is fixed) from its histidine tail is ∼40 Å.[45−47] This should result in a separation distance of ∼70−71 Å, which is in very good agreement with the average value reported in Table 3. Good agreement is also observed for the 510 nm emitting QD−Cy3 pair, where the anticipated distance from geometrical considerations (using a QD size of 25 Å) is

~65−66 Å.[45−47] However, the distances deduced from geometrical considerations for the 530 nm QDs and Cy3 pair (with a QD radius of 28 Å) are larger than those reported in Table 3 using the donor quenching ($r \approx 67-68$ Å versus 61−62 Å extracted from donor quenching data). Note that the agreement between the Cy3 integrated PL increase shown in Figure 3 and the values expected from the donor quenching is good for all QD−Cy3 pairs studied. However, agreement between values for the separation distances extracted from donor quenching and those from geometrical considerations are good only for 510 and 555 nm QD conjugates. Distances derived from FRET data are smaller than those measured by SAXS and TEM for the sample of 530 nm QDs. A lower efficiency is thus required to provide distances comparable to those estimated from structure measurements (SAXS and TEM): efficiency varies as $1/r^6$. More precisely, a slightly smaller efficiency (e.g., 0.65 for 10 acceptors, which represents ~84% of what was reported) would be needed to provide an average separation distance of 67−68 Å.

The higher FRET efficiency measured for the 530 QD samples may *a priori* be surprising. This sample has the lowest quantum yield and the longest exciton lifetime of the three sets of solutions studied (Tables 1 and 2). However, a longer exciton decay lifetime would also make nonradiative energy transfer compete more efficiently with the donor excitation decay via radiative and nonradiative channels than in a system having shorter exciton lifetimes. This can potentially produce a higher FRET signal for a donor having lower QY. The lower photoluminescence QY and the slightly longer lifetime for this sample may be caused by surface defects, either within the inorganic structure or at the interface with the organic ligands. It can be attributed to the initial preparation conditions for the QDs. Such problems are known to affect QDs prepared by wet chemistry solutions techniques, as small but nonnegligible fluctuations in the photoemission efficiency of QD dispersions are observed for these colloidal inorganic fluorophores.[25,26]

It is important to note that the advantage of using donor quenching results to calculate FRET efficiency derives primarily from its simplicity: the signal does not need to be adjusted by other measured parameters. Conversely, acceptor enhancement requires additional adjustment to account for direct excitation and estimates of the extinction coefficients of both fluorophores (see below). However, gain in acceptor fluorescence represents directly the energy transferred nonradiatively from the donor that contributed to acceptor emission, with no regard to non-FRET sources of donor quenching. Under ideal conditions where every exciton is nonradiatively transferred to an acceptor, FRET would imply that donor photoemission loss is fully recovered as energy gain by the acceptor.

We now discuss the use of two alternative treatments (to donor quenching) of the data to extract estimates for the separation distance r_n. In the first treatment, we analyze changes in the donor exciton lifetime upon interactions with acceptor(s) and use an alternative expression for the FRET efficiency,[7,8,48]

$$E = 1 - \frac{\tau_{DA}}{\tau_D} \tag{9}$$

where τ_{DA} is the fluorescence lifetime of the donor in the presence of the acceptor and τ_D is the fluorescence lifetime of the donor alone. This expression is essentially a restatement of eq 7 and constitutes a replicate measurement of distance using donor fluorescence data. Using the lifetime results from Table 2, we calculated donor−acceptor distances for all QD−Cy3 pairs (results are shown in Table 3). These values are close to those deduced from the QD PL loss. This is not surprising since the analysis focuses on changes in the QD donor exciton behavior during interactions with the acceptor(s) and should be associated with the donor PL loss. Nonetheless, a ~5 Å mismatch between the data extracted from the donor quenching and the fluorescence lifetime data is measured for the 555 nm QD−Cy3 pair, a result that can be attributed to the strong overlap between QD and dye emissions, which made a complete separation and analysis of the donor decay signal difficult. We should emphasize that using 10 MBPs instead 15 to prepare the conjugates for the lifetime experiments does not affect the comparison, as data for QD−15MBP and QD−10MBP conjugates provided similar values for τ_D and Q_D. Both ratios of MBP to QD provided PL enhancement near the saturation regime.[21,42]

The second analysis is based on using the enhanced acceptor fluorescence signal instead of the donor quenching, where an alternative expression for the FRET efficiency, defined as[7]

$$E = \frac{\epsilon_A(\lambda_{ex})F_{AD}}{\epsilon_D(\lambda_{ex})F_A} \tag{10}$$

(in place of eq 7), is used to determine donor−acceptor distances from the Cy3 PL enhancement; F_{AD} is the acceptor fluorescence upon interacting with a donor, corrected for direct excitation, and $\epsilon_A(\lambda_{ex})$ and $\epsilon_D(\lambda_{ex})$ are, respectively, the extinction coefficients of the acceptor and donor at the excitation wavelength λ_{ex}. Equation 10 indicates that accurate estimates of donor and acceptor extinction coefficients are required when using the acceptor signal as a means of calculating distances. This limitation is notably absent when using the donor quenching analysis. Substituting this definition into eq 8 and solving for r_n should provide a new set of values for the separation distances for the three QD-dye pairs to be compared with structural analyses. However, QD extinction coefficients are inherently difficult to determine due to uncertainties in the sample concentration.[49] These are typically estimated from absorption data and comparison to the growth solution, assuming a near 100% yield in the reaction (i.e., all organometallic precursors are consumed in the reaction leading to nanocrystal growth)[26] which often underestimates the QD extinction coefficient. To reduce the effects of uncertainties in $\epsilon_A(\lambda_{ex})$ and $\epsilon_D(\lambda_{ex})$ on the analysis, we employed an alternative approach where the ratio $\epsilon_A(\lambda_{ex})/\epsilon_D(\lambda_{ex})$ in eq 10 was treated as a fitting parameter with an initial value equal to the one measured from absorption data.[26] Using this approach, we found that there is an optimum value

(45) Mattoussi, H.; Cumming, A. W.; Murray, C. B.; Bawendi, M. G.; Ober, R. *Phys. Rev. B* **1998**, *58*, 7850−7863.
(46) Murray, C. B. Ph.D. Dissertation, Massachusetts Institute of Technology, 1995.
(47) (a) Chang, H. C.; Bao, Z.; Yao, Y.; Yse, A. G.; Goyarts, E. C.; Madsen, M.; Kawasaki, E.; Brauer, P. P.; Sacchattini, J. C.; Nathenson, S. G.; Reinherz, E. L. *Proc. Natl. Acad. Sci. U.S.A.* **1994**, *91*, 11408−11412. (b) O'Shea, E. K.; Lumb, K. J.; Kim, P. S. *Curr. Biol.* **1993**, *3*, 658−667 and references therein.
(48) Michalet, X.; Pinaud, F.; Lacoste, T. D.; Dahan, M.; Bruchez, M. P.; Alivisatos, A. P.; Weiss, S. *Single Molecules* **2001**, *2*, 261−276.
(49) Leatherdale, C. A.; Woo, W.-K.; Mikulec, F. V.; Bawendi, M. G. *J. Phys. Chem. B* **2002**, *106*, 7619−7622.

for $\epsilon_A(\lambda_{ex})/\epsilon_D(\lambda_{ex})$ that provided a near constant value for distances r_n over the entire range of the dye/QD ratios used for each QD−Cy3 pair. The resulting distance values were very close to those derived from donor quenching and lifetime data for the three donor−acceptor pairs (i.e., $\langle r_n \rangle \approx 65$ Å, 60 Å, and 70 Å for 510, 530, and 555 nm emitting QDs, respectively; see Table 3). Any small variation in the ratio $\epsilon_A(\lambda_{ex})/\epsilon_D(\lambda_{ex})$ resulted in a rapidly diverging trend for r_n (see the Supporting Information). As expected, the values for the fitted extinction coefficient ratio were close but slightly and consistently smaller than those determined from experimental absorption data (see the Supporting Information). While a fitting procedure is not typically desirable, uncertainties in the extinction ratio are inherently large and the subsequent fitting results are strikingly consistent with donor-based measurements of the separation distance. This agreement between donor and acceptor-based measurements further confirms that a FRET process is the dominant factor in the above observations where most of the QD energy loss is translated into Cy3 PL gain.

The present study differs significantly from previously reported QD-based FRET studies in several important ways.[50,51] Here, the fluorescent acceptor dye has been covalently attached at a known site in an engineered, well-characterized protein. This provided good control over the separation distances involved (within the range of 50−100 Å where FRET interactions are most effective), as well as the number of dye-labeled proteins in each QD conjugate. The protein immobilization on the QD donor center (via self-assembly) is stable and reproducible. Furthermore, additional tests such as measurements of changes in the exciton lifetime upon conjugate formation, variation in the spectral overlap integral, and their effects on the data were examined. In the previous reports, inclusion of an intermediate protein between the QD and the acceptor resulted in separation distances too large to produce significant FRET signals. Furthermore, control over the number and exact location of the acceptors in those QD conjugates was difficult to realize.

Finally, we discuss several properties that make QD fluorophores uniquely suited for developing QD conjugate nanosensor assemblies based on FRET assays. In addition to being able to control the overlap integral by size tuning the photoemission, it is also possible to increase the effective FRET cross section (via a linear manipulation of the overlap integral) by attaching two or more dyes to the same donor. This can eventually allow one to utilize acceptors with a modest degree of spectral overlap and yet achieve a substantial rate of FRET, resulting in a large acceptor emission. Furthermore, it is possible to realize a configuration where more than one type of acceptor-labeled protein can interact with the same QD center and potentially achieve multicolor FRET. This configuration has large potential in developing multianalyte-sensing devices, where two, three, or even four types of receptor proteins are immobilized on the QD surface and interact with several target analytes. We are presently undertaking studies of these model sensors.

Conclusions

We have used QD bioconjugates as energy donors in a FRET binding assay, where properties such as size tuning of the spectral overlap integral and FRET cross section via titration of the number of acceptor dyes interacting with a single QD donor are explored. Samples consisted of Cy3-labeled MBP proteins that have been immobilized via a noncovalent self-assembly process onto surface functionalized QDs. We observed a progressive and substantial enhancement in the energy transfer efficiency with increasing number of MBP−Cy3 attached to a single nanocrystal, for a given population of QDs, or with increasing the degree of spectral overlap for a given acceptor dye. Fluorescence lifetime measurements provided additional proof confirming that FRET was the dominant mechanism. Using Förster theory, we were able to extract measurements of the average donor−acceptor separation distance for each QD−dye pair and found that, in general, distance measurements varied proportionally with average QD core size from one set of conjugates to another.

These results provided in-depth analysis of a QD−protein bioconjugate FRET system and demonstrated the utility of QDs as efficient energy donors. The ability of tuning (via size) the nanocrystal photoemission properties should allow for efficient energy transfer with a number of conventional organic dyes. Furthermore, the large size of QD fluorophores compared to organic dyes allowed design of a sample configuration where multiple acceptors could interact with a single donor, which enhances FRET signals and thus measurement sensitivity. This suggests the possibility of realizing multiple analyte detection using a single QD donor. However, we anticipate that there will be some limitations to using longer wavelength emitting QDs (e.g., emission maximum > 600 nm) as FRET donors due to larger core sizes and lower quantum yields. Similarly, FRET based assays using QD bioconjugates will require careful preparation of intermediary proteins, polysaccharides, or oligonucleotides in order to ensure sufficient signal change upon acceptor binding. Receptor−ligand binding selectivity as well as donor−acceptor binding proximity will be vital to realizing an efficient and accurate assay.

Acknowledgment. We thank H. Hellinga (Duke University) for providing the plasmid with the MBP-his-tagged gene sequence utilized. A.R.C. and I.L.M. acknowledge National Research Council Fellowships. J.M.M. and H.M. thank K. Ward at the Office of Naval Research (ONR) for research support, Grant N001400WX20094. B.R.F. acknowledges the National Defense Science and Engineering Graduate Fellowship Program for support.

Supporting Information Available: One figure showing the effect of fitting distance data from acceptor-based efficiencies and one table showing all measured efficiency data. This material is available free of charge via the Internet at http://pubs.acs.org.

JA037088B

(50) Willard, D. M.; Carillo, L. L.; Jung, J.; Van Orden, A. *Nano Lett.* **2001**, *1*, 469−474.
(51) Wang, S.; Mamedova, N.; Kotov, N. A.; Chen, W.; Studer. J. *Nano Lett.* **2002**, *2*, 817−822.